

# Asynchronous Bioplausible Neuron for Spiking Neural Networks for Event-Based Vision

Sanket Kachole<sup>1</sup> Hussain Sajwani<sup>2,3</sup> Fariborz Baghaei Naeini<sup>1</sup> Dimitrios Makris<sup>1</sup> Yahya Zweiri<sup>2,3</sup>

**Abstract**—Spiking Neural Networks (SNNs) offer a biologically inspired approach to computer vision that can lead to more efficient processing of visual data with reduced energy consumption. However, maintaining homeostasis within these networks is challenging, as it requires continuous adjustment of neural responses to preserve equilibrium and optimal processing efficiency amidst diverse and often unpredictable input signals. In response to these challenges, we propose the Asynchronous Bioplausible Neuron (ABN), a dynamic spike firing mechanism to auto-adjust the variations in the input signal. Comprehensive evaluation across various datasets demonstrates ABN’s enhanced performance in image classification and segmentation, maintenance of neural equilibrium, and energy efficiency.

## I. INTRODUCTION

Computer vision has experienced significant success over recent years due to the advancement of Artificial Neural Networks such as Convolutions Neural Networks (CNNs) and Vision Transformers. In recent years, the attraction of Spiking Neural Networks (SNNs) has been growing, due to their potential in real-time sensory processing, closer imitation of biological brain functionalities, and low power consumption. The advent of event-based cameras further accelerates this evolution, offering a promising path to harness the strengths of SNNs and address the challenges faced by traditional vision systems. This combination paves the way for more energy-efficient and adaptive solutions in computer vision [1].

SNNs’ performance benefits from homeostasis, i.e. maintaining a stable neuron activity level, neither spiking too often nor staying too quiet [2]–[4]. To achieve this, standard methods adjust parameters like fixed firing thresholds or synaptic weights. These strategies require fine-tuning, and may not be versatile across network architectures. The fixed thresholds in spiking neurons, as shown in Fig. 1, can be sensitive to initial conditions, leading networks to be overly active or dormant. The inflexibility in adapting to varying inputs makes neurons either too sensitive or unresponsive, affecting negatively the performance. It also compromises energy efficiency, with either high power usage from excessive firing or missed data from sparse firing.

To address the above challenges, we introduce the Asynchronous Bioplausible Neuron (ABN) function, which can be incorporated into the two most prominent bioplausible neuron models: the Spike Response Model (SRM) [5] and the Leaky Integrate-and-Fire (LIF) model [6]. We validate the effectiveness of our approach using two SNNs for object segmentation and image classification tasks under both normal and various degraded conditions, such as low light, high occlusion etc. Further our method has been tested on five different datasets:

N-MNIST [7], ESD-1, ESD-2 [8], DVS128-Gesture [9], and CIFAR-10 DVS [10] to demonstrate its general applicability across various tasks. Additionally, we conducted an extensive study of the homeostasis (i.e. stability test of neuron firing), an ablation study to understand the impact of elements of the proposed function and compared the power consumption with state-of-the-art methods. The contributions of this research are as follows:

- 1) The main contribution of the research is to propose a novel function for dynamic Spike Firing Limits within neuron models of SNNs that utilizes weighted factors including Membrane Gradient (MG) for Spike Frequency Adaptation, Threshold Retrospective Gradient (TRG) for Burst Suppression and Spike Efficiency (SE) for Homeostasis as shown in Fig. 2.
- 2) We demonstrate the practical application of the ABN in image classification and object segmentation, particularly on asynchronous event-based visual data.

The remainder of this paper is structured as follows: Section II discusses related work, Section III details the proposed methodology, Section IV presents experimental results, and Section V concludes and discusses future research.

## II. RELATED WORK

### A. Computer vision applications of SNNs

The exploration of SNNs for object segmentation and image classification has ignited widespread interest in the field, as the SNNs replicate the biological neuronal system to provide efficient and effective solutions for this task. Initial works in object segmentation leaned on feed-forward SNN architectures, utilizing the spike-timing-dependent plasticity (STDP) learning rule for unsupervised learning of features [11]. The Backpropagation Through Time (BPTT) method introduced in [12] for training SNNs, offers a more structured and supervised learning approach that significantly enhances feature extraction and classification accuracy, yet it is limited by its high computational complexity, substantial memory requirements, susceptibility to vanishing and exploding gradients, challenges in capturing long-term dependencies, and inefficiency in real-time learning applications. The introduction of Convolutional Spiking Neural Networks (CSNNs) marked a significant development in image classification. By incorporating convolutional layers into the network, these models could better handle the spatial complexities inherent in images, significantly enhancing segmentation performance. Concurrently, they maintained the temporal dynamics native to SNNs, enabling efficient processing of streaming data [13].

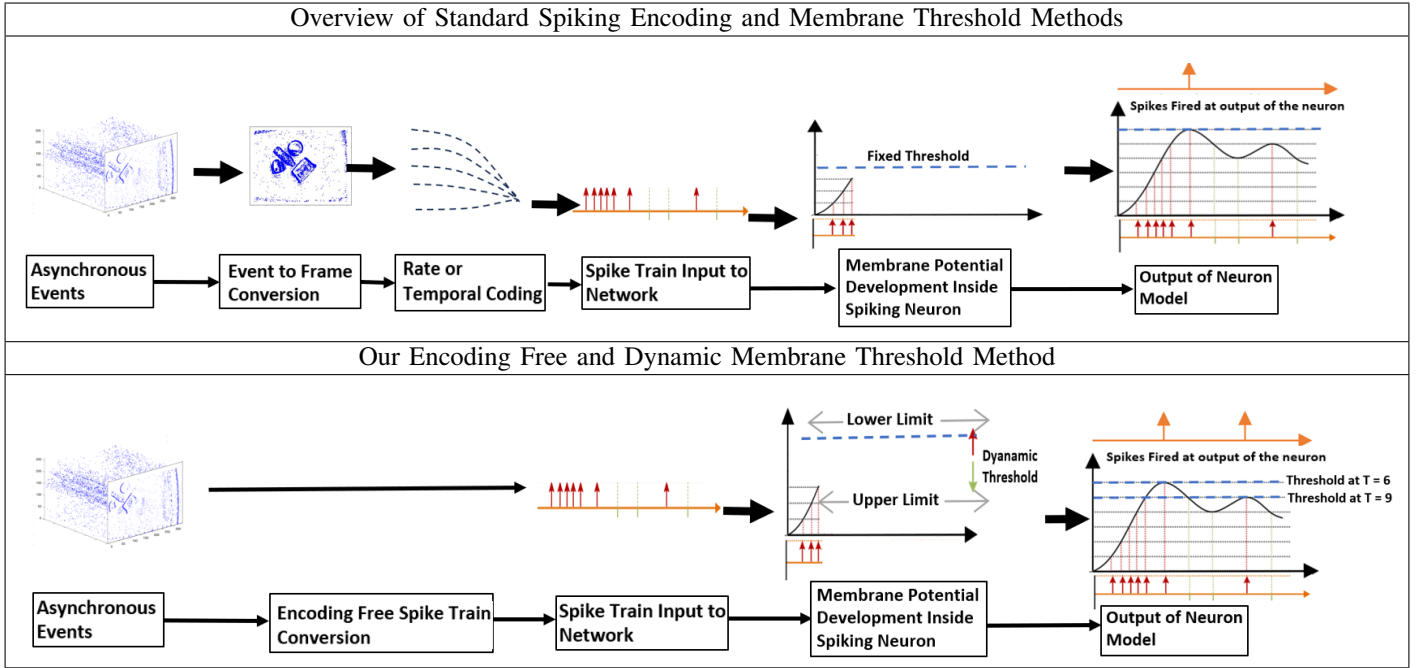


Fig. 1: Comparative Visualization of SNNs approaches: The top image presents the overview of the SNN methodology showcasing the conventional processes of asynchronous event capture, event-to-frame conversion, and fixed thresholding in neuronal spike response. In contrast, the bottom image illustrates an overview of the proposed method, highlighting the the explicit encoding of events to spikes and implementing a dynamic thresholding mechanism for neuronal spiking. This juxtaposition underscores the novel methodology proposed.

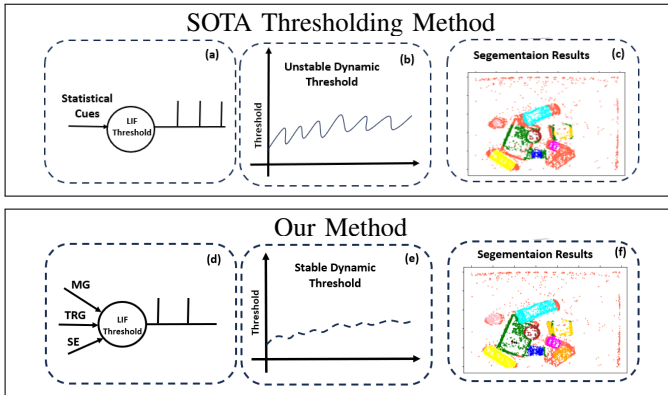


Fig. 2: Dynamic thresholding techniques for SNNs: Existing methods are based on the LIF neuron which uses statistical cues for thresholding (a), however they result in unstable thresholds (b) and consequently low accuracy for segmentation methods (c). Our proposed method incorporates weighted inputs in the form of MG, TRG, and SE (d), which results in a smoothed dynamic threshold (e), and improved segmentation (f).

Recently, there has been a surge in the application of recurrent spiking neural networks (RSNNs) to image classification. These networks leverage feedback connections, enhancing the network’s ability to capture temporal dependencies in the data. Furthermore, their capacity to retain information over extended periods makes them particularly suited to segmentation tasks involving sequential or video data [14].

### B. Dynamic Thresholding in SNNs

Research on SNNs has delved deeply into dynamic thresholding methods to bolster adaptability. For instance, while predictive coding emphasizes anticipating input patterns, it overlooks the spike timing significance, an aspect STDP-based adjustments address [15], [16]. The holistic approach of network activity regulation contrasts with the inherent refractory period modulation, focusing on preventing rapid neuron firing [17]. Furthermore, spiking models like SRM and LIF have advanced neuron dynamics representations [18], [19]. However, gaps remain, especially in dynamic threshold modulation. [20] introduced a method utilizing a scaling factor to adjust the threshold in response to increased input. Yet, since it was tailored specifically for incremental spike membrane potential, it faltered when faced with variations in membrane decays. On the other hand, [21] adopted exponential functions to dictate decay. This approach, however, resulted in fluctuating thresholding levels, failing to ensure a smooth threshold curve. Meanwhile, [22] ventured into a firing counter-based threshold adjustment. This method, while innovative, necessitated meticulous fine-tuning and exhaustive experimentation, leaving the determination of an optimal count mired in ambiguity.

Clearly, the previous research may not addressed all the dynamics in the input signal, especially in highly complex event-based vision signal. In event-based vision, SNNs face unique challenges: Neurons within the same layer exhibit varying event counts; some neurons experience more events than others. Consequently, applying BDETT method [23],

which utilizes average membrane potential of the neurons in a layer to predict the threshold of all the neurons in that layer, does not accurately reflect the individual dynamics of each neuron. This paper addresses notable research gaps. No prior studies have demonstrated that a bioinspired dynamic threshold can stabilize spike firing in semantic segmentation tasks. Additionally, these studies typically employ simplistic datasets such as MNIST [7] and rarely evaluate system robustness under challenging conditions like motion blur or low light, vital for assessing the system's homeostasis [24].

### III. METHODOLOGY

#### A. Pre-requisite

Event-based vision cameras are designed to register variations in logarithmic light intensities by recording individual pixel-level changes, referred to as events. These events generate a continuous event stream, which can be mathematically articulated as a series of ordered tuples. A tuple corresponds to an event  $i$  and includes its spatial coordinates  $(x_i, y_i)$ , temporal stamps  $t_i$ , and polarity value  $z_i$  [25]:

$$(x_1, y_1, t_1, z_1), (x_2, y_2, t_2, z_2), \dots, (x_n, y_n, t_n, z_n) \quad (1)$$

The LIF model, as shown in Fig. 1, is characterized by its linear integration of inputs until a threshold  $\Theta(t)$  is reached, causing its firing [6]. Mathematically, the sub-threshold dynamics of the membrane potential  $V(t)$  of an LIF neuron can be described by the following differential equation:

$$\tau_m \frac{dV(t)}{dt} = -(V(t) - E_L) + R_m I(t) \quad (2)$$

$\tau_m$  is the membrane time constant that dictates the speed at which the neuron responds to inputs,  $E_L$  is the leak potential or resting potential representing the equilibrium potential of the neuron in the absence of any input,  $R_m$  is the membrane resistance, and  $I(t)$  represents the total synaptic input to the neuron that might come from other neurons or external sources. When the membrane potential  $V(t)$  reaches the threshold  $\Theta(t)$ , the neuron emits a spike and then resets its potential to a reset value  $V_{\text{reset}}$ , typically below  $\Theta(t)$ . Additionally, after spiking, the neuron enters a refractory period for a duration  $T_{\text{ref}}$  during which it cannot fire again. The "leaky" aspect of the LIF model comes from the term  $(V(t) - E_L)$  in the differential equation. This term ensures that in the absence of any input, the neuron's potential will gradually revert to the leak potential  $E_L$ .

In the SRM [5], incoming spike trains  $s_i(t)$  are initially transformed into a spike response signal by convolving them with a spike response kernel  $\varepsilon(\cdot)$ , denoted as  $(\varepsilon * s_i)(t)$ . Subsequently, this spike response signal is scaled by a synaptic weight  $w_i$ . The depolarization process involves summing up these scaled spike response signals across all incoming spikes, mathematically represented as  $\sum_i w_i (\varepsilon * s_i)(t)$ . The SRM also incorporates a mechanism for hyperpolarization when a spike  $s(t)$  is triggered. This is characterized by a refractory potential  $(\zeta * s)(t)$ , where  $\zeta(\cdot)$  serves as the refractory kernel. This dual-component approach enables SRM to capture both excitatory and inhibitory dynamics in neuronal spike activity.

#### B. Asynchronous Bioplausible Neuron

1) *Asynchronous events to spike conversion*: Traditionally, rate coding and temporal coding [26], [27] are the popular methods to convert the frames into spiking inputs to SNN. However, event data can be directly treated as spikes which helps to avoid the requirement to convert the input signal into a spike train. In [28] this study, each event is treated as a spike. Each pixel on the sensor corresponds to a neuron in the SNN, and that neuron fires a spike at the times when the pixel generates an event. This approach essentially uses a form of temporal coding, because the information is conveyed through the timing of the spikes. In this study, we have chosen to drop the polarity aspect of the events due to its high sensitivity, which can introduce noise and complicate the signal processing. Mathematically,  $E(t)$  is the event stream,  $e = (x, y, t)$  is an individual event with coordinates  $x$ ,  $y$  and timestamp  $t$ , and  $S_i(t)$  is the spike train for the  $i$ -th neuron:

$$S_i(t) = \begin{cases} \delta(t - e_t) & \text{if } e_x = x_i \text{ and } e_y = y_i \\ 0 & \text{otherwise} \end{cases} \quad (3)$$

Here,  $\delta(t - e_t)$  is the Dirac delta function, which generates a "spike" at the time of the event.

2) *Asynchronous Bioplausible Neuron (ABN)*: The proposed ABN is a weighted combination of the Membrane Gradient (MG), Threshold Retrospective Gradient (TRG), and Spike Efficiency (SE) for threshold adjustment, uniquely tailored for each neuron. This individualization is crucial as each neuron receives a unique frequency of events, necessitating adaptation to input variations and ensuring the maintenance of firing stability, irrespective of the layer. Each component of the ABN is detailed in the subsequent subsections: III-B3, III-B4, and III-B5. The mathematical equation of the ABN is:

$$\Theta_i(t + 1) = \Theta_i(t) + k_1 MG_i - k_2 TRG_i + k_3 SE_i \quad (4)$$

The equation models the dynamic adjustment of the neuron's firing threshold at the next time step  $t + 1$  based on various factors. In this equation,  $\Theta(t)$  is the existing threshold at time  $t$ , and  $k_1, k_2, k_3$  are weights that determine the relative influence of each term. The term  $k_1 \cdot MG_i$  increases the threshold when the membrane potential is rapidly changing, preventing the neuron from firing too easily. Conversely, the term  $-k_2 \cdot TRG_i$  decreases the threshold if there has been a historical trend of rapid threshold increases. Lastly, the term  $k_3 \cdot SE_i$  takes into account the neuron's recent spiking activity. Specifically, if the neuron is overly active, this term will make it more difficult for the neuron to fire in the future, thereby ensuring efficiency. Overall, this equation encapsulates a multi-faceted approach to dynamically adapting the neuron's firing threshold.

3) *Membrane Gradient (MG)*: The rate of change of the membrane potential is a critical parameter for predicting a dynamic threshold in SNNs. It serves as an indicator of the neuron's responsiveness to incoming spikes and plays an essential role in governing the neuron's firing behavior. Positive correlations between dynamic thresholds and membrane potentials have been observed in several areas of diverse

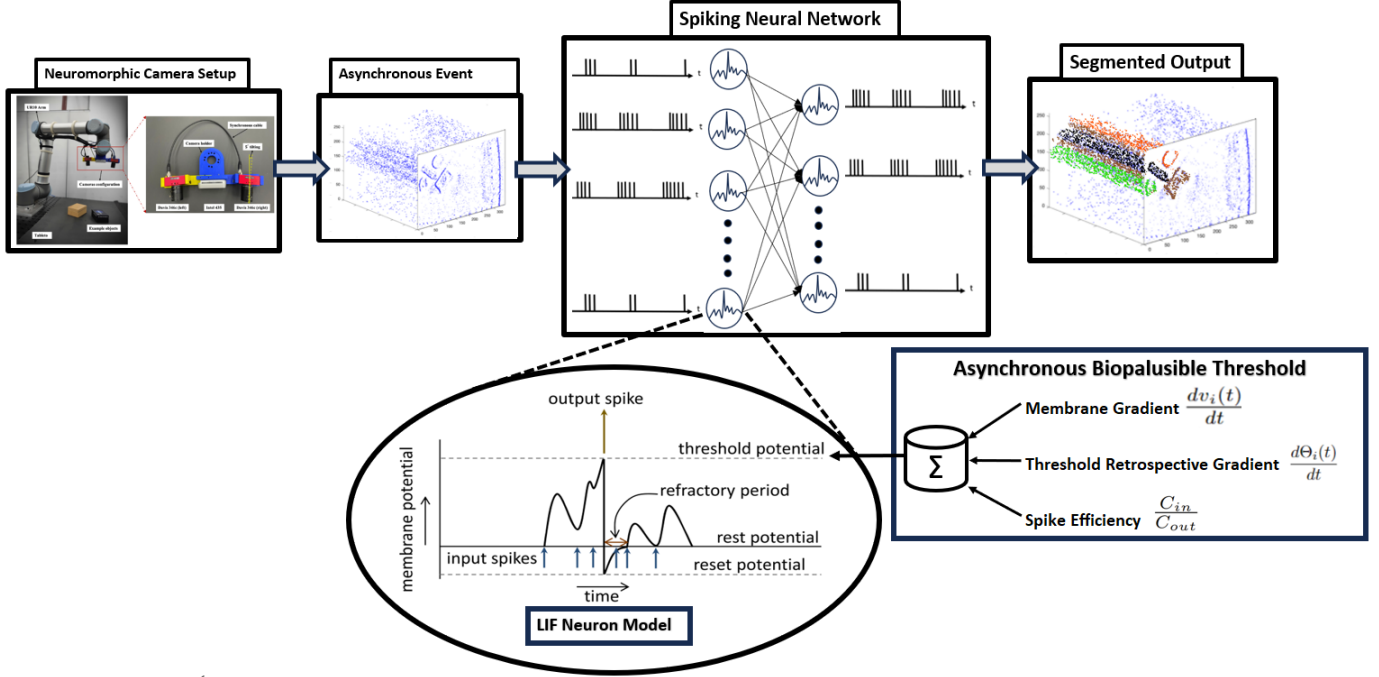


Fig. 3: Schematic Diagram of ABN. The DVS camera outputs data in the form of asynchronous events. It is passed into a SNN with neurons in the first layer equal to the number of pixels on the camera. Each neuron adopts the proposed ABN where it takes the weighted input from the MG, TRG, and SE to control the dynamic threshold.

biological nervous systems. In [29], the average membrane potential is correlated with an average threshold to predict the dynamic threshold. Instead, in this work we correlate the rate of change of membrane potential with a threshold. A high rate of change often signifies that the neuron is receiving a burst of spikes, necessitating a higher threshold to maintain neuronal homeostasis. Conversely, a lower rate of change could indicate that the neuron is less active, allowing for a lower dynamic threshold to be sensitive to sparse inputs. Incorporating the rate of change of the membrane potential into the calculation of a dynamic threshold ensures that the SNNs can adapt to varying synaptic activities, thereby emulating the adaptability and energy efficiency observed in biological neurons.

The BDETT method presented in [23] considers the statistical cues of the membrane potential, whereas, in this work we adopt the derivative term, denoted as  $\eta \cdot \frac{dv_i(t)}{dt}$ , which captures the rate of change of membrane potential of neuron  $i$  at time  $t$ , denoted by  $v_i(t)$ . To numerically compute the derivative, a finite difference approximation is employed. This involves the subtraction of the membrane potential at the previous timestep from the current potential, followed by division by the timestep size  $\Delta t$ . The scaling factor  $\eta$ , which is set to a value less than 1, reduces the rate of change to ensure that the rate of change of the threshold remains less than the rate of change of the potential. The explicit equation for the derivative term is given as:

$$MG_i = \frac{dv_i(t)}{dt} \approx \frac{v_i(t) - v_i(t-1)}{\Delta t} \quad (5)$$

4) *Threshold Retrospective Gradient (TRG)*: Biological systems exhibit a negative correlation with the preceding rate

of depolarization, which indicates the excitatory status. We propose considering a historical rate of change for the threshold  $\Theta(t)$ . This is because focusing solely on the preceding rate of depolarization as implemented in [23] may be insufficient and can result in an unstable or overly sensitive dynamic threshold. Therefore, we take into account the average of the historical rate of change of the dynamic threshold. Utilizing the historical rate of change of the dynamic threshold to calculate the current threshold can provide the neuron with an inertia or memory of its past states. This can be useful in situations where the neuron should react not only based on the current state but also considering its past behavior.

In discrete terms, if  $\Theta(t)$  is the threshold at time  $t$ , then the rate of change at  $t$  is:

$$G_i(t) = \frac{\Theta_i(t) - \Theta_i(t-1)}{\Delta t} \quad (6)$$

The historical rate of change is an average of these rates over a recent window of time,  $N$  time steps:

$$\bar{G}_i(t) = \frac{1}{N} \sum_{j=0}^{N-1} G_i(t-j) \quad (7)$$

In order to ensure that the older rates influence the current threshold less within the sliding window, a decay factor  $\alpha$ , ( $0 < \alpha < 1$ ), is used:

$$TRG_i = \frac{1}{N} \sum_{j=0}^{N-1} \alpha^j G_i(t-j) \quad (8)$$

with values closer to 0 suppressing more the older rates.

In summary, leveraging the historical rate of change of the dynamic threshold has introduced a form of temporal inertia to the neuron, creating a relationship to patterns in input data over time. Importantly, it is especially useful in scenarios where temporal patterns are crucial.

5) *Spike Efficiency (SE)*: The ratio of spike output  $C_{\text{out}}$  to spike input  $C_{\text{in}}$  can serve as a crucial metric for determining the dynamic threshold in a SNN. Intuitively, this ratio indicates how efficiently a neuron is converting incoming spikes into outgoing spikes. A high SE suggests that the neuron is highly responsive to incoming activity, and could therefore benefit from a lower dynamic threshold to maintain energy efficiency and reduce the likelihood of over-saturation. Conversely, a low SE implies that the neuron is less responsive, possibly requiring a higher dynamic threshold to avoid unnecessary firing and thereby preserve neuronal and computational resources. This ratio is mathematically represented as:

$$r_i(t) = \frac{C_{\text{out},i}(t)}{C_{\text{in},i}(t)} \quad (9)$$

When using a sliding window method, we only consider  $N$  previous time steps to calculate  $C_{\text{in}}$  and  $C_{\text{out}}$ . This allows the threshold to adapt quickly to recent changes in spike rates.

$$SE_i = \bar{r}_i(t) = \frac{\sum_{j=t-N}^t C_{\text{out},i}(j)}{\sum_{j=t-N}^t C_{\text{in},i}(j)} \quad (10)$$

Incorporating SE into the dynamic threshold calculation enables the SNN to adjust its sensitivity according to the context of incoming activity. This inclusion ensures a more nuanced and adaptive network behavior, aligning closely with biological plausibility while maintaining computational efficiency. It allows the network to operate in a balanced regime, irrespective of the incoming spike rates, ensuring robust and stable performance across different input conditions. This adaptive mechanism is invaluable, especially when individual neurons within a network necessitate autonomous regulation of their activity, contingent on their functional significance or the unique input patterns they discern.

## IV. RESULTS

### A. Experimental Protocol

We assess the effectiveness of the proposed ABN in two Computer Vision tasks: Image Classification for the N-MNIST [30], CIFAR10-DVS [10], DVS128 gesture recognition [9] datasets, and Object Semantic Segmentation for the ESD-1 [8] and ESD-2 [8] datasets. The details of the datasets are explained in supplementary section B. The Spiking MLP employs Spatio-Temporal Backpropagation [23] for training, allowing the network to consider both spatial and temporal information during the learning process. Although the input to the first layer should be a spike train, we can directly use asynchronous event-based vision data without requiring specific conversion. The initialization of network parameters, such as weights and thresholds, is crucial for stabilizing the network’s firing activities. We adopt the initialization strategy as discussed in [31]. In order to make a fair comparison with

TABLE I: Classification and Segmentation Accuracy across Various Datasets and Models

Method	Classification						Segmentation			
	N-MNIST		DVS128		CIFAR10		ESD-1		ESD-2	
Spiking RBM [33]	92.1	93.16	87.38	90.21	83.04	86.25	48.95	51.05	45.2	50.31
Spiking MLP (BP) [34]	94.52	97.66	90.72	93.4	86.23	90.06	49.53	54	45.5	52.42
Spiking MLP (STDP) [35]	93.47	95	90.8	92.01	87.5	91.7	52.63	58.84	46.7	49.44
Spiking MLP (STBP) [31]	97.13	98.89	92.54	93.64	86.23	91.73	55.82	63.09	49.07	51.37
DT1 [36]	99.05	99.4	95.01	96.88	89.17	92.65	57.55	61.45	50.13	54.59
DT2 [22]	98.13	98.24	92.54	95.54	89.38	91.47	58.28	64.3	53.49	56.5
BDETT [23]	99.15	99.45	94.09	96.05	91.61	93.5	61.02	65.39	51.36	55.46
ABN (Ours)	<b>99.23</b>	<b>99.48</b>	<b>95.64</b>	<b>98.74</b>	<b>93.5</b>	<b>94.74</b>	<b>61.56</b>	<b>67.29</b>	<b>56.23</b>	<b>58.04</b>

[23], we have used similar experimental configuration. The model was trained on a GPU PC featuring 128GB of memory, an Intel Xeon W-2155 Processor, and NVIDIA Quadro RTX 8000 48GB graphics cards, housed in a Lenovo ThinkStation P520. While this is essential for assessing the efficacy of the proposed method, implementing it directly on neuromorphic hardware may require additional engineering efforts, which are beyond the scope of this work. We conducted experiments using the `snn-torch` [32] package and 0.7.0 version. Custom code was written to develop the LIF and SRM within this framework. Synaptic weights are initialized randomly, and a decay constant,  $\tau_1$ , is set to 0.1 ms. The weights for constants  $K1$ ,  $K2$ , and  $K3$  are experimentally selected as 0.25, 0.50, and 0.25, respectively (see section IV-F).

### B. Comparative Results across Diverse Datasets

The evaluation of our ABN method’s generalization capabilities, across diverse datasets and neuron models is shown in Table I. Performance on the classification datasets was evaluated using classification accuracy and on the object segmentation using event accuracy. The metrics are detailed in the supplementary document section C. On the N-MNIST dataset, ABN achieved the highest classification accuracy (**99.23%** with SRM and **99.48%** with LIF), surpassing other methods like BDETT and DT1. In the ESD-1 and ESD-2 datasets, designed for robotic grasping tasks: ABN again outperformed others, showing particularly strong performance in the ESD-2 dataset with unknown objects (**56.23%** with SRM and **58.04%** with LIF). For the DVS128 Gesture and CIFAR10-DVS datasets, ABN recorded the highest scores (**95.64%** and **98.74%** with SRM and LIF in DVS128; **93.5%** and **94.74%** in CIFAR10-DVS), indicating its robustness and effectiveness. This comprehensive performance underscores the superior adaptability and effectiveness of the ABN method across a variety of datasets and computer vision tasks.

### C. Evaluation on Degraded Input on ESD-1

We conducted an experiment focused on evaluating the segmentation performance of various state-of-the-art methods, and compared them to our proposed ABN, under conditions of degraded inputs. This experiment was essential to mirror real-world scenarios affected by factors like low light, occlusion, variations in speed and distance from the object, and the direction of camera motion. These factors significantly impact the quality of input, making it crucial to determine the robustness of the proposed method in less-than-ideal conditions. Utilizing the ESD-1 dataset, we measured the

TABLE II: Segmentation accuracy of known objects in various conditions.

Exp 1: varying clutter objects, Bright light, 62cm height, Rotational motion, 0.15 m/s speed					
Method	2 Obj	4 Obj	6 Obj	8 Obj	10 Obj
Spiking MLP (STBP) [31]	74.16%	73.05%	66.79%	66.42%	54.42%
DT1 [36]	77.56%	74.65%	68.20%	68.70%	55.49%
DT2 [22]	78.46%	75.42%	69.28%	69.62%	56.16%
BDETT [23]	79.07%	78.03%	74.14%	69.83%	58.28%
ABN (ours)	<b>81.49%</b>	<b>79.74%</b>	<b>74.97%</b>	<b>72.16%</b>	<b>60.03%</b>
Exp 2: 6 Objects, varying lighting conditions, 62cm height, Rotational Motion, 0.15 m/s speed.					
Method	Bright Light	Low light			
Spiking MLP (STBP) [31]	58.73%	61.59%			
DT1 [36]	61.32%	62.91%			
DT2 [22]	61.24%	64.53%			
BDETT [23]	63.92%	66.03%			
ABN (Ours)	<b>65.98%</b>	<b>67.42%</b>			
Exp 3: 6 Objects, Bright Light, 62cm height, Varying directions of motion, 0.15 m/s speed.					
Method	Linear	Rotational	Partial Rotational		
Spiking MLP (STBP) [31]	48.09%	63.99%	67.43%		
DT1 [36]	49.09%	65.14%	69.31%		
DT2 [22]	50.43%	66.89%	69.79%		
BDETT [23]	52.09%	68.60%	72.04%		
ABN (Ours)	<b>55.50%</b>	<b>69.45%</b>	<b>73.54%</b>		
Exp 4: 6 Objects, Bright Light, 62cm height, Rotational motion, Varying speed.					
Method	0.15 m/s	0.3 m/s	0.1 m/s		
Spiking MLP (STBP) [31]	53.16%	68.12%	56.29%		
DT1 [36]	54.56%	70.27%	60.16%		
DT2 [22]	55.27%	72.31%	59.63%		
BDETT [23]	56.67%	75.09%	63.16%		
ABN (Ours)	<b>59.63%</b>	<b>76.72%</b>	<b>63.56%</b>		
Exp 5: 6 Objects, Bright Light, Varying camera height, Rotational motion, Varying speed.					
Method	62 cm	82 cm			
Spiking MLP (STBP) [31]	62.93%	55.05%			
DT1 [36]	63.82%	59.08%			
DT2 [22]	65.63%	59.93%			
BDETT [23]	65.82%	59.00%			
ABN (ours)	<b>68.40%</b>	<b>63.27%</b>			

event accuracy to gauge the performance. The results across various conditions, as depicted in Table II, consistently show that the ABN method outperforms all other SNN methods in all tested scenarios. Clearly, the superior ability of ABN to maintain high segmentation accuracy despite the challenging input conditions, confirms its efficacy and potential for real-world applications.

#### D. Homeostasis Evaluation

Homeostasis in SNNs is crucial as it reflects the network’s ability to maintain stable internal conditions despite external environmental variations. It is an important indicator of the network’s reliability and efficiency, especially when dynamic input is considered.

In an experimental setup across all variations of the ESD-1 dataset, various statistical indicators were used to quantify the homeostasis of the host SNNs. Specifically, for a fair comparison with [23] we employed  $FR_m$ ,  $FR_m\_std$ , and  $FR_s\_std$  metrics, representing the average neuron firing rate over all trials, the mean of standard deviations of neuron firing rates over individual trials, and the variability of these standard deviations, respectively. Our proposed ABN model demonstrates significantly lower values across all three metrics and all conditions. These results suggest a stable and well-regulated network, highlighting the ABN model’s capacity for homeostasis.

#### E. Ablation Study - Spike Activity Analysis

The ablation study of the proposed ABN model, focused on the distinct behaviors of its constituent elements MG,

TABLE III: Homeostasis Performance on ESD-1 Known Object

	$FR_m$	$\Delta FR_m$	$FR_m\_std$	$\Delta FR_m\_std$	$FR_s\_std$	$\Delta FR_s\_std$
Spiking MLP (STBP) [31]	0.631		0.485		0.001564	
DT1 [36]	0.524		0.459		0.001146	
DT2 [22]	0.507		0.416		0.000983	
BDETT [23]	0.436		0.403		0.001224	
ABN (Ours)	<b>0.385</b>		<b>0.253</b>		<b>0.000891</b>	
Spiking MLP (STBP) [31]	0.783	0.152	0.582	0.097	0.001396	0.000168
DT1 [36]	0.692	0.168	0.561	0.102	0.003963	0.002817
DT2 [22]	0.586	0.079	0.484	0.068	0.002724	0.001741
BDETT [23]	0.47	0.034	0.357	0.046	0.002291	0.001067
ABN (Ours)	<b>0.373</b>	<b>0.012</b>	<b>0.291</b>	<b>0.038</b>	<b>0.000784</b>	<b>0.000107</b>
Spiking MLP (STBP) [31]	0.786	0.155	0.594	0.109	0.003942	0.002378
DT1 [36]	0.698	0.174	0.405	0.054	0.002508	0.001362
DT2 [22]	0.594	0.087	0.489	0.073	0.003641	0.002658
BDETT [23]	0.498	0.062	0.467	0.064	0.001157	0.000067
ABN (Ours)	<b>0.405</b>	<b>0.02</b>	<b>0.295</b>	<b>0.042</b>	<b>0.000889</b>	<b>0.00002</b>
Spiking MLP (STBP) [31]	0.746	0.115	0.582	0.097	0.001666	0.000102
DT1 [36]	0.62	0.096	0.406	0.053	0.001167	0.000021
DT2 [22]	0.609	0.102	0.351	0.065	0.002839	0.001856
BDETT [23]	0.517	0.081	0.352	0.051	0.002077	0.000853
ABN (Ours)	<b>0.305</b>	<b>0.08</b>	<b>0.206</b>	<b>0.047</b>	<b>0.000881</b>	<b>0.00001</b>
Spiking MLP (STBP) [31]	0.701	0.07	0.505	0.02	0.003798	0.002334
DT1 [36]	0.601	0.077	0.409	0.05	0.003461	0.002315
DT2 [22]	0.415	0.092	0.397	0.019	0.002827	0.001844
BDETT [23]	0.395	0.041	0.351	0.052	0.00133	0.000106
ABN (Ours)	<b>0.378</b>	<b>0.007</b>	<b>0.243</b>	<b>0.01</b>	<b>0.000875</b>	<b>0.000016</b>
Spiking MLP (STBP) [31]	0.759	0.128	0.533	0.048	0.003901	0.002337
DT1 [36]	0.675	0.151	0.449	0.01	0.002263	0.001117
DT2 [22]	0.551	0.044	0.45	0.034	0.001346	0.000363
BDETT [23]	0.481	0.045	0.354	0.049	0.002763	0.001539
ABN (Ours)	<b>0.373</b>	<b>0.012</b>	<b>0.255</b>	<b>0.002</b>	<b>0.000879</b>	<b>0.000012</b>

TABLE IV: Performance Analysis for different values of K1, K2, and K3, using CIFAR and DVS128.

	K1	K2	K3	CIFAR		DVS128	
				Acc.	F. Rate	Acc.	F. Rate
0.05	0.15	0.05	67.39	0.841	69.34	0.872	
0.15	0.25	0.15	86.71	0.625	91.02	0.713	
0.25	0.5	0.25	<b>94.74</b>	<b>0.352</b>	<b>97.83</b>	<b>0.421</b>	
0.5	0.75	0.5	61.82	0.936	76.48	0.947	
0.75	0.85	0.75	52.01	1.62	57.01	1.707	

TRG, and SE, observed across the CIFAR-10 DVS, ESD-2, and DVS-128 Gesture Recognition datasets, as depicted in Fig. 4. The MG demonstrated a robust increase in firing rates over time, while the TRG exhibited an inverse trend, decreasing over the same intervals. These opposing dynamics suggest that while each element responds distinctly to temporal stimuli, they collectively contribute to a regulatory effect, mitigating abrupt fluctuations and promoting threshold stability in the ABN model. The SE component further modulates this balance, optimizing the firing rates for computational efficiency. In addition, the variability in the firing rate patterns across different datasets reflects the distinct event frequencies encountered within each dataset. The CIFAR-10 DVS dataset, with its more uniform event timing, facilitates a steady increase in the MG’s influence, whereas the ESD-2’s irregular events lead to more erratic firing rates, challenging threshold stabilization. The DVS-128 Gesture Recognition dataset, with its complex event sequences, showcases the ABN model’s adaptability to rapid temporal changes. This highlights the ABN model’s capacity to modulate neural firing in response to the diverse temporal structures of sensory input.

#### F. Ablation Study - Weighting Factor Selection

This study aims to experimentally select the weighting factors K1, K2, and K3, which correspond to the three elements

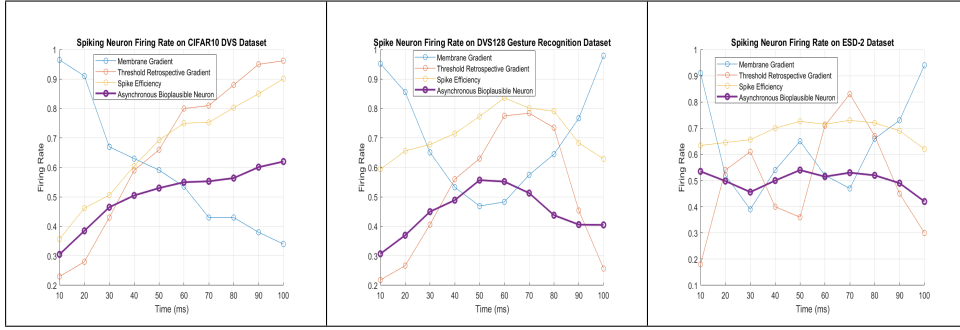


Fig. 4: Ablation Study Spike Activity Analysis of each element of the ABN

of the ABN. The experiment utilized the CIFAR-DVS and DVS128 datasets for gesture recognition to determine the optimal combination of K1, K2, and K3. This was achieved by evaluating the combinations through metrics of image classification accuracy and firing rate. It was observed that as the combination of K1, K2, and K3 started from 0.05, 0.15, and 0.05 respectively and incrementally increased, the accuracy of image classification improved. Peak performance and the lowest firing rates were achieved at the combination of K1=0.25, K2=0.5, and K3=0.25. Beyond this point, further increases in the K values led to a decrease in accuracy and a surge in firing rates. Therefore, having identified the optimal combination, it becomes crucial to examine the most influential element of the ABN, which is the focus of the subsequent subsection.

### G. Ablation Study - ABN Analysis

TABLE V: Ablation Study of the ABN

Feat.	Params			CIFAR		DVS128	
	K1	K2	K3	Acc.	FR	Acc.	FR
MG	0.25	0	0	74.48	0.534	79.41	0.682
TRG	0	0.5	0	83.03	0.516	87.34	0.603
SE	0	0	0.25	56.35	0.832	61.4	0.854
MG+TRG	0.25	0.5	0	78.52	0.523	82.01	0.671
TRG+SE	0	0.5	0.25	81.3	0.481	84.01	0.601
MG+SE	0.25	0	0.25	59.26	0.704	63.28	0.853
All	<b>0.25</b>	<b>0.5</b>	<b>0.25</b>	<b>94.74</b>	<b>0.352</b>	<b>97.83</b>	<b>0.421</b>

This ablation study, as presented in Table V, examines the individual and combined contributions of each functional element (MG, TRG, SE) to the overall performance on the CIFAR and DVS128 datasets. The results clearly indicate that all three factors- MG, TRG, and SE are crucial, as each one independently enhances performance. Specifically, the integration of TRG demonstrates the most significant impact on performance, followed by MG and SE, in terms of their contribution to the final outcomes. When these elements are synergistically combined using the weights K1, K2 and K3 selected from the previous study (section IV-G), the model achieves its peak performance, with a classification accuracy of 94.74% on CIFAR and 97.83% on DVS128. Moreover, an inverse relationship between firing rate and accuracy is evident, especially in the full ABN model. This is exemplified by the model achieving the highest accuracy with the lowest firing

rates of 0.352 on CIFAR and 0.421 on DVS128, indicating an efficient utilization of spikes for enhanced accuracy.

### H. Energy Consumption

Table VI presents an analysis of power consumption, comparing CNN, SotA SNNs and the ABN using the DVS128 hand gesture recognition dataset. As proposed in [24], MAC (Multiply-Accumulate operations) and AC (Accumulate Count) were used to calculate power consumption. Details are described in supplementary document.

Methods by [37] and [38], employing CNN models, show a higher power consumption of 0.541W and 1.56W, respectively, despite their zero AC. In contrast, the SNN models [24], demonstrate significantly lower power usage, with hybrid and SNN models consuming 0.404W and 0.053W, respectively. BDETT's [24] SNN model further reduces this consumption to 0.046W. Notably, our proposed SNN model outperforms these by achieving the lowest power consumption of just 0.038W, even with a higher AC of 105, underscoring the efficiency of our model in terms of energy usage compared to both CNNs and other SNNs.

TABLE VI: Power Consumption Comparison

Method	Model	MAC	AC	Power (W)
Calabrese [37]	CNN	285	0	0.541
Baldwin [38]	CNN	963	0	1.56
Asude [24]	Hybrid	235	81	0.404
Asude [24]	SNN	0.6	123	0.053
BDETT [24]	SNN	0.7	115	0.046
Ours	SNN	<b>0.4</b>	105	<b>0.038</b>

## V. CONCLUSION

This paper introduces the Asynchronous Bioplausible Neuron (ABN) within a spiking multi-layer perceptron (MLP). This innovative spiking neuron incorporates a dynamic threshold based on Membrane Gradient (MG) for Spike Frequency Adaptation, Threshold Retrospective Gradient (TRG) for Burst Suppression, Spike Efficiency (SE) for Homeostasis. The spiking MLP, which utilizes STDP, serves as the architecture for implementing the proposed neuron.

A methodology for object segmentation and image classification that employs a dynamic vision sensor and the ABN is also proposed. Remarkably, this system can directly process asynchronous, event-based vision signals without requiring

any preprocessing. Its performance was rigorously evaluated on both conventional datasets (N-MNIST, DVS128 Gesture, and CIFAR10-DVS) and specialized robotic grasping datasets (ESD-1, ESD-2). The method achieved state-of-the-art performance in terms of classification accuracy and event-wise accuracy across different degraded signal conditions. Additionally, our approach has demonstrated excellent homeostatic properties, maintaining stable neuronal firing rates under challenging conditions such as occlusions, low light levels, the presence of small or rapidly moving objects, and linear motion. Notably, it also exhibited the lowest power consumption among the models evaluated.

Future work in this area could aim to further approximate the characteristics of real human neurons and enhance the biological plausibility of the system. There are multiple ways to implement dynamic thresholds, and combining several of these into a single function could be a promising avenue for future research. Specific aspects that could be incorporated include the dynamic refractory period, the temporal distance between consecutive spikes, and overall network activity.

## REFERENCES

- [1] N. Rathi, I. Chakraborty, A. Kosta, A. Sengupta, A. Ankit, P. Panda, and K. Roy, "Exploring Neuromorphic Computing Based on Spiking Neural Networks: Algorithms to Hardware," *ACM Computing Surveys*, vol. 55, no. 12, pp. 1–49, 12 2023.
- [2] K. Pozo and Y. Goda, "Unraveling Mechanisms of Homeostatic Synaptic Plasticity," *Neuron*, vol. 66, no. 3, pp. 337–351, 5 2010.
- [3] T. Cazalets and J. Dambre, "An homeostatic activity-dependent structural plasticity algorithm for richer input combination," in *2023 International Joint Conference on Neural Networks (IJCNN)*. IEEE, 6 2023, pp. 1–8. [Online]. Available: <https://ieeexplore.ieee.org/document/10191230/>
- [4] L. C. Yeung, H. Z. Shouval, B. S. Blais, and L. N. Cooper, "Synaptic homeostasis and input selectivity follow from a calcium-dependent plasticity model," *Proceedings of the National Academy of Sciences*, vol. 101, no. 41, pp. 14943–14948, 10 2004.
- [5] W. Gerstner, "Time structure of the activity in neural network models." *Physical review. E, Statistical physics, plasmas, fluids, and related interdisciplinary topics*, vol. 51, no. 1, pp. 738–758, 1 1995.
- [6] W. Gerstner and W. M. Kistler, *Spiking Neuron Models*. Cambridge: Cambridge University Press, 8 2002.
- [7] G. Orchard, A. Jayawant, G. K. Cohen, and N. Thakor, "Converting Static Image Datasets to Spiking Neuromorphic Datasets Using Saccades," *Frontiers in Neuroscience*, vol. 9, 2015. [Online]. Available: <https://www.frontiersin.org/articles/10.3389/fnins.2015.00437>
- [8] X. Huang, K. Sanket, A. Ayyad, F. B. Naeini, D. Makris, and Y. Zweiri, "A Neuromorphic Dataset for Object Segmentation in Indoor Cluttered Environment," 2 2023. [Online]. Available: <http://arxiv.org/abs/2302.06301>
- [9] A. Amir, B. Taba, D. Berg, T. Melano, J. McKinstry, C. Di Nolfo, T. Nayak, A. Andreopoulos, G. Garreau, M. Mendoza, J. Kusnitz, M. Debole, S. Esser, T. Delbruck, M. Flickner, and D. Modha, "A Low Power, Fully Event-Based Gesture Recognition System," in *2017 IEEE Conference on Computer Vision and Pattern Recognition (CVPR)*. IEEE, 7 2017, pp. 7388–7397.
- [10] H. Li, H. Liu, X. Ji, G. Li, and L. Shi, "CIFAR10-DVS: An Event-Stream Dataset for Object Classification," *Frontiers in Neuroscience*, vol. 11, 5 2017.
- [11] M. Deng and C. Li, "STDP and Competition Learning in Spiking Neural Networks and its application to Image Classification," in *2021 International Conference on Information, Cybernetics, and Computational Social Systems, ICCSS 2021*. Institute of Electrical and Electronics Engineers Inc., 2021, pp. 385–389.
- [12] Y. Kim, J. Chough, and P. Panda, "Beyond classification: directly training spiking neural networks for semantic segmentation," *Neuromorphic Computing and Engineering*, vol. 2, no. 4, p. 44015, 12 2022. [Online]. Available: <https://dx.doi.org/10.1088/2634-4386/ac9b86>
- [13] J. Li, H. Zhang, R. Wu, Z. Zhu, L. Chen, Z. Zheng, B. Wang, and C. Meng, "A Graph is Worth 1-bit Spikes: When Graph Contrastive Learning Meets Spiking Neural Networks," 5 2023. [Online]. Available: <http://arxiv.org/abs/2305.19306>
- [14] T. Bohnstingl, A. Surina, M. Fabre, Y. Demirag, C. Frenkel, M. Payvand, G. Indiveri, and A. Pantazi, "Biologically-inspired training of spiking recurrent neural networks with neuromorphic hardware," in *2022 IEEE 4th International Conference on Artificial Intelligence Circuits and Systems (AICAS)*. IEEE, 6 2022, pp. 218–221.
- [15] R. P. N. Rao and D. H. Ballard, "Predictive coding in the visual cortex: a functional interpretation of some extra-classical receptive-field effects," *Nature Neuroscience*, vol. 2, no. 1, pp. 79–87, 1999. [Online]. Available: <https://doi.org/10.1038/4580>
- [16] "High Accuracy Implementation of Adaptive Exponential Integrated and Fire Neuron Model," *IEEE World Congress on Computational Intelligence*, p. 5301, 2016.
- [17] L. Wang, J. C. Rajapakse, K. Fukushima, S.-Y. Lee, X. Yao, M. Yoshida, and H. Hayashi, "Regulation of Spontaneous Rhythmic Activity and Preserved Stimulus Dependent Pattern by STDP in the Hippocampal CA3 Model," Tech. Rep.
- [18] W. Gerstner, "Time structure of the activity in neural network models," *Physical Review E*, vol. 51, no. 1, pp. 738–758, 1 1995.
- [19] W. Gerstner and W. M. Kistler, "Spiking Neuron Models: Single Neurons, Populations, Plasticity," 8 2002.
- [20] Y. Hao, X. Huang, M. Dong, and B. Xu, "A Biologically Plausible Supervised Learning Method for Spiking Neural Networks Using the Symmetric STDP Rule," 12 2018.
- [21] A. Shaban, S. S. Bezugam, and M. Suri, "An adaptive threshold neuron for recurrent spiking neural networks with nanodevice hardware implementation." *Nature communications*, vol. 12, no. 1, p. 4234, 7 2021.
- [22] T. Kim, S. Hu, J. Kim, J. Y. Kwak, J. Park, S. Lee, I. Kim, J.-K. Park, and Y. Jeong, "Spiking Neural Network (SNN) With Memristor Synapses Having Non-linear Weight Update." *Frontiers in computational neuroscience*, vol. 15, p. 646125, 2021.
- [23] J. Ding, B. Dong, F. Heide, Y. Ding, Y. Zhou, B. Yin, and X. Yang, "Biologically Inspired Dynamic Thresholds for Spiking Neural Networks," *Neural Information Processing Systems*, 2022.
- [24] A. Aydin, M. Gehrig, D. Gehrig, and D. Scaramuzza, "A Hybrid ANN-SNN Architecture for Low-Power and Low-Latency Visual Perception," 3 2023.
- [25] P. Lichtsteiner, C. Posch, and T. Delbruck, "A 128 × 128 120 dB 15 μs latency asynchronous temporal contrast vision sensor," *IEEE Journal of Solid-State Circuits*, vol. 43, no. 2, pp. 566–576, 2 2008.
- [26] Y. Kim, H. Park, A. Moitra, A. Bhattacharjee, Y. Venkatesha, and P. Panda, "Rate Coding or Direct Coding: Which One is Better for Accurate, Robust, and Energy-efficient Spiking Neural Networks?" *ICASSP, IEEE International Conference on Acoustics, Speech and Signal Processing - Proceedings*, vol. 2022-May, pp. 71–75, 2022.
- [27] H. M. Lehmann, J. Hille, C. Grassmann, and V. Issakov, "Spiking Neural Networks based Rate-Coded Logic Gates for Automotive Applications in BiCMOS," in *2021 IEEE International Conference on Microwaves, Antennas, Communications and Electronic Systems, COMCAS 2021*. Institute of Electrical and Electronics Engineers Inc., 2021, pp. 280–285.
- [28] S. Abreu, M. Gouda, A. Lugnan, and P. Bienstman, "Flow cytometry with event-based vision and spiking neuromorphic hardware," in *2023 IEEE/CVF Conference on Computer Vision and Pattern Recognition Workshops (CVPRW)*. IEEE, 6 2023, pp. 4139–4147.
- [29] B. Fontaine, J. L. Peña, and R. Brette, "Spike-threshold adaptation predicted by membrane potential dynamics in vivo." *PLoS computational biology*, vol. 10, no. 4, p. e1003560, 4 2014.
- [30] G. Orchard, A. Jayawant, G. K. Cohen, and N. Thakor, "Converting static image datasets to spiking neuromorphic datasets using saccades," *Frontiers in neuroscience*, vol. 9, p. 437, 2015.
- [31] Y. Wu, L. Deng, G. Li, J. Zhu, and L. Shi, "Spatio-Temporal Back-propagation for Training High-Performance Spiking Neural Networks," *Frontiers in Neuroscience*, vol. 12, 5 2018.
- [32] J. K. Eshraghian, M. Ward, E. O. Neftci, X. Wang, G. Lenz, G. Dwivedi, M. Bennamoun, D. S. Jeong, and W. D. Lu, "Training Spiking Neural Networks Using Lessons From Deep Learning," *Proceedings of the IEEE*, vol. 111, no. 9, pp. 1016–1054, 9 2023. [Online]. Available: <https://snntorch.readthedocs.io/en/latest/#>
- [33] E. Neftci, S. Das, B. Pedroni, K. Kreutz-Delgado, and G. Cauwenberghs, "Event-driven contrastive divergence for spiking neuromorphic systems," *Frontiers in Neuroscience*, vol. 7, 2014.
- [34] P. O'Connor and M. Welling, "Deep Spiking Networks," *arXiv*, 2 2016.



- [35] P. Ferré, F. Mamalet, and S. J. Thorpe, “Unsupervised Feature Learning With Winner-Takes-All Based STDP,” *Frontiers in Computational Neuroscience*, vol. 12, 4 2018.
- [36] Y. Hao, X. Huang, M. Dong, and B. Xu, “A Biologically Plausible Supervised Learning Method for Spiking Neural Networks Using the Symmetric STDP Rule,” 12 2018.
- [37] E. Calabrese, G. Taverni, C. A. Easthope, S. Skriabine, F. Corradi, L. Longinotti, K. Eng, and T. Delbruck, “DHP19: Dynamic Vision Sensor 3D Human Pose Dataset,” in *2019 IEEE/CVF Conference on Computer Vision and Pattern Recognition Workshops (CVPRW)*, 2019, pp. 1695–1704.
- [38] R. W. Baldwin, R. Liu, M. Almatrafi, V. Asari, and K. Hirakawa, “Time-Ordered Recent Event (TORE) Volumes for Event Cameras,” *IEEE Transactions on Pattern Analysis and Machine Intelligence*, vol. 45, no. 2, pp. 2519–2532, 2 2023.